Optical and acoustic plasmons in cylindrical quantum-well wires

L. Wendler and V. G. Grigoryan

Fachbereich Physik, Martin-Luther-Universität Halle, Friedemann-Bach-Platz 6, D-06108 Halle, Federal Republic of Germany
(Received 1 March 1993; revised manuscript received 21 December 1993)

We study theoretically the collective electronic excitations of quasi-one-dimensional cylindrical quantum-well wires, the intrasubband and intersubband plasmons in the random-phase approximation. Using a two-subband model we calculate the dispersion curves for the case that two subbands are occupied. We study the influence of the image forces on the intrasubband and intersubband plasmons in detail. These modes are split in two branches. The intrasubband plasmon branches can be classified in an optical and an acoustic branch which are influenced quite differently by the image forces. The intersubband plasmon branches behave like acoustic plasmons.

I. INTRODUCTION

The enormous progress in epitaxial-layer growth techniques and high-resolution submicrometer technologies has given another dimension in the study of the semiconductor systems. With these techniques the artificial realization of low-dimensional electron systems, from three dimensions to quasi-zero-dimensions (Q0D), is possible.

In quasi-one-dimensional (Q1D) quantum-well wires (QWW) the electron motion is only free in one spatial direction, but quantum confined in the two other spatial directions. The spectrum of the single particle as well as of the collective excitations depends characteristically on the dimensionality of the system. The most prominent collective excitation of modulation-doped semiconductor nanostructures is the plasmon and, if a magnetic field is applied, the magnetoplasmon. Plasmons and magnetoplasmons have been explored experimentally[1-6] and theoretically without[7-21] and with magnetic field[22-25] in isolated QWW's and lateral multiwire superlattices. The theoretical works on Q1D plasmons predict, according to the size quantization, two different types of excitations, intrasubband plasmons which are connected with electron motion within one subband, and intersubband plasmons which are connected with electron motion between two different subbands.

Most of the theoretical works were done using the random-phase approximation (RPA) to calculate the linear response of the quasi-one-dimensional electron gas (Q1DEG) to an external charge.[7-19,21-25] It was shown[7,26] that the intrasubband plasmon shows a logarithmic dispersion $\omega \propto |\mathbf{q}| a[-\ln(|\mathbf{q}| a)]^{1/2}$ for small one-dimensional wave vectors $|\mathbf{q}|$. The constant a depends on the wire size and is equal to the width of a rectangular potential,[7] to the radius of a cylindrical potential,[10] or to the characteristic width of a parabolic potential.[16] The first quantum theory of intersubband plasmons was presented by Que and Kirczenow.[8] Intersubband plasmons in QWW's are investigated in detail by Li and Das Sarma,[14] Hu and O'Connell,[16] and Wendler and co-workers.[15,17-19]

For the case where more than one electric subband is occupied Li and Das Sarma,[14] Que,[12] and Wendler

et al.[15] investigated the intrasubband plasmons using quantum-mechanical linear response theory in the RPA. Wendler et al.[15] showed that the intrasubband plasmons of the higher occupied subbands exist in gaps between the single-particle intrasubband continua and are free of Landau damping. Exploring intersubband plasmons in QWW's for the case if more than one subband is occupied, it was shown by Wendler et al.[15] and Mendoza and Schaich[13] that in the additional regions, which are between the single-particle intersubband continua and free of Landau damping, new additional branches of intersubband plasmons exist.

For an initial parabolic potential (bare potential) it was shown in Ref. 19 by performing self-consistent calculations of the ground-state and the linear response of the Q1DEG that the lowest intersubband plasmon has for small wave vectors a frequency nearly identical with the bare harmonic oscillator frequency, and independent of the density of the Q1DEG. This is a result of the generalized Kohn theorem.[27] Further, the influence of retardation effects on Q1D plasmons was investigated recently.[20]

A far-infrared (FIR) transmission experiment was carried out by Hansen et al.[1] In this paper it was found that the intersubband resonance frequency has a large depolarization shift, also measured in the experiments of Brinkop et al.[2] and Demel et al.[3] In a recent FIR transmission experiment Drexler et al.[4] showed that the principal collective intersubband resonance is "split" in three modes above and below the frequency $\omega = \sqrt{2}\,\omega_c$ ($\omega_c = eB/m_e$: cyclotron frequency) at a higher gate bias. A FIR transmission experiment on plasmons and magnetoplasmons propagating along the wire axis was performed by Demel et al.[3] Plasmons[5] and magnetoplasmons[6] of the Q1DEG have been detected also in resonant inelastic light scattering.

The theoretical model calculations mostly involve the rectangular or parabolic shape of the confining potential in lateral direction but assume a confinement in the growth direction of the semiconductor sample of zero thickness. The model of a cylindrical confining potential has the advantage considering the finite width of the QWW in both spatial directions. Hence this model is a good approximation for experimentally used QWW's

<u>49</u>   14 531

in which the width of the confining potential is nearly the same for both spatial directions. The density response is considered for a Q1DEG confined in cylindrical quantum-well wires[10,11,28] (CQWW) and hollow cylinders.[29-34] In these papers the collective excitations in the absence[10,11,28-32] and in the presence of an axial magnetic field[30,33,34] are discussed and investigated within the RPA. It is shown[11,29] that for a plasma mode the collective electron transitions between subbands with equal difference of the angular quantum number are coupled, but are decoupled from such electron transitions with a different difference of the angular quantum number. Further, Q1D plasmons in CQWW's have a spectrum periodic with the magnetic field.[33] The collective excitations of a paraxial ring superlattice are investigated in Ref. 34. Different types of plasmons and magnetoplasmons are found.

The model of a CQWW has further the advantage of deriving in many cases analytical expressions.[10,35] Experimental observations by Merkt[36] indicate the importance of the image contributions, especially for the depolarization shift of the intersubband plasmons. The cylindrical symmetry allows one to calculate the influence of the image forces present in semiconductor structures realized from different semiconductor materials having different polarizabilities. The results obtained until now on Q1D plasmons in CQWW's (Refs. 10 and 11) to the case where only the lowest subband is occupied, neglecting the effects of the image forces on the plasmons. However, QWW's with many occupied subbands are used mostly in experiments.[1-6,36]

Many properties of Q1D plasmons and magnetoplasmons are investigated. But some questions remain open, e.g., (i) is the Q1DEG better described as a Fermi liquid, or is the model of a Tomonaga-Luttinger liquid more appropriate? (ii) What is the physical origin of the $\sqrt{2}\,\omega_c$ "splitting" in the spectrum of Q1D magnetoplasmons? (iii) What is the physical nature of the Q1D plasmon modes if more than one subband is occupied? (iv) What is the influence of the image forces on the Q1D plasmons?

The *aim* of this paper is to give an answer to the two last questions. In this paper we present a quantum theory of Q1D plasmons in CQWW's within the RPA for the case of two occupied subbands including the effect of the image potential. Further, we investigate the physical nature of the resulting modes in detail.

II. GROUND STATE

The model used in this paper is the following. The electrons are totally confined in an effective potential with cylindrical shape of radius R in the x-y plane and are free to move along the axis of the wire of length L_z which we assume to be the z axis. The single-particle Schrödinger equation reads

$$\left\{ -\frac{\hbar^2}{2m_e}\left[\frac{1}{r}\frac{\partial}{\partial r}\left(r\frac{\partial}{\partial r}\right) + \frac{1}{r^2}\frac{\partial^2}{\partial \varphi^2}\frac{\partial^2}{\partial z^2}\right] + V_{\text{eff}}(r)\right\}$$

$$\times \Psi_{mlk_z}(\mathbf{x}) = \mathcal{E}_{ml}(k_z)\Psi_{mlk_z}(\mathbf{x}), \quad (1)$$

where we use cylindrical coordinates (r, φ, z), suppose

spin degeneracy, but omit the spin eigenvalue and coordinate for simplicity. Because of the translational symmetry in z direction (Born–von Kármán boundary conditions) the single-particle wave function and the corresponding eigenvalues are given by

$$\langle \mathbf{x} | mlk_z \rangle = \Psi_{mlk_z}(\mathbf{x}) = \frac{1}{\sqrt{2\pi L_z}}e^{i(m\varphi + k_z z)}\kappa_{ml}(r) \quad (2)$$

and

$$\mathcal{E}_{ml}(k_z) = \mathcal{E}_{ml} + \frac{\hbar^2 k_z^2}{2m_e}, \quad m = 0, \pm 1, \pm 2, \ldots, \quad l = 1, 2, 3 \quad (3)$$

with

$$\kappa_{ml}(r) = \sqrt{\frac{2}{R^2}}\,\frac{1}{J_{|m|+1}(k_{|m|l}R)}J_{|m|}(k_{|m|l}r), \quad (4)$$

$$\mathcal{E}_{ml} = \frac{\hbar^2 k_{|m|l}^2}{2m_e}. \quad (5)$$

In these equations m_e is the effective conduction-band edge mass and k_z is the wave vector component in z direction. The energy levels are twofold degenerated ($\mathcal{E}_{ml} = \mathcal{E}_{-ml}$) if $m \neq 0$. In Eq. (4) $J_{|m|}(k_{|m|l}r)$ is the Bessel function of order $|m|$, m is the angular quantum number, and l is the radial quantum number. The radial quantum number l is equal to the number of zeros of the radial wave function $\kappa_{ml}(r)$ in the interval $(0, R]$ and $k_{|m|l}$ is related to the lth root of the Bessel function of order $|m|$, i.e., $J_{|m|}(k_{|m|l}R) = 0$ resulting from the boundary condition $\Psi_{mlk_z}(r = R, \varphi, z) = 0$. Thus the subband ladder is $\mathcal{E}_{01} < \mathcal{E}_{11} < \mathcal{E}_{21} < \mathcal{E}_{02} < \mathcal{E}_{31} < \mathcal{E}_{12} < \mathcal{E}_{41} < \mathcal{E}_{03}\ldots$.

Because it is our goal in this paper to investigate the physical nature of the modes if two subbands are occupied including the effect of the image potential, we have to derive some analytical results. As shown by Gold and Ghazali,[10] the use of the following expressions of the normalized single-particle wave functions for the lowest subbands:

$$\kappa_{01}(r) = \frac{\sqrt{6}}{R}\left[1 - \left(\frac{r}{R}\right)^2\right], \quad (6)$$

$$\kappa_{\pm 11}(r) = \frac{2\sqrt{6}}{R}\left(\frac{r}{R}\right)\left[1 - \left(\frac{r}{R}\right)^2\right], \quad (7)$$

results in a very good agreement with the exact result, Eq. (4), if one calculates the bare electron-electron interaction potential. For the analytical calculations we will use these wave functions.

III. DENSITY RESPONSE OF A Q1DEG

In this section we calculate the linear response of a Q1DEG to an external potential on a quantum-mechanical level within the RPA, also known as the time-dependent Hartree method. There are different methods to develop the RPA. Here we use the self-consistent field (SCF) method of Ehrenreich and Cohen.[37]

The single-particle Hamiltonian of the electrons of the

Q1DEG in the presence of the perturbation is written as $H(\mathbf{x}, t) = H_0(\mathbf{x}) + V^{\mathrm{SC}}(\mathbf{x}, t)$, where H_0 is the unperturbed Hamiltonian of a single electron confined in the CQWW satisfying $H_0|m, l, k_z\rangle = \mathcal{E}_{ml}(k_z)|m, l, k_z\rangle$ and $V^{\mathrm{SC}}(\mathbf{x}, t)$ is the self-consistent potential which is a sum of the external potential $V^{\mathrm{ext}}(\mathbf{x}, t)$ and the induced potential $V^{\mathrm{ind}}(\mathbf{x}, t)$. The total electron number density of the Q1DEG $n = n_0 + n_{\mathrm{ind}}$ is a sum of the ground-state electron number density (equilibrium) n_0 and the induced electron number density n_{ind}. Writing the statistical operator ρ_G as $\rho_G^{(0)} + \rho_G^{(1)}$, where $\rho_G^{(0)}$ is the statistical operator of the unperturbed system and $\rho_G^{(1)}$ is the correction to the statistical operator to the first order in the perturbation, we have $n_{\mathrm{ind}}(\mathbf{x}, \omega) = \mathrm{Tr}\{\rho_G^{(1)}\delta(\mathbf{x} - \mathbf{x}_e)\}$. Using a general state $|\nu\rangle$ of the unperturbed system, where $\{\nu\}$ stands for $\{m, l, k_z\}$, the induced electron number density is given by

$$n_{\mathrm{ind}}(\mathbf{x}, \omega) = \sum_\nu n_{\mathrm{ind}}^{(\nu)}(\mathbf{x}, \omega) = \sum_\nu \langle \nu | \rho_G^{(1)} \delta(\mathbf{x} - \mathbf{x}_e) | \nu \rangle,$$
$$(8)$$

where $n_{\mathrm{ind}}^{(\nu)}(\mathbf{x}, \omega)$ is the induced electron number density of the state $|\nu\rangle$. Standard linear response theory relates n_{ind} to the self-consistent potential by the equation

$$n_{\mathrm{ind}}(\mathbf{x}, \omega) = \int d^3x' P^{(1)}(\mathbf{x}, \mathbf{x}'|\omega) V^{\mathrm{SC}}(\mathbf{x}', \omega),$$
$$(9)$$

where

$$P^{(1)}(\mathbf{x}, \mathbf{x}'|\omega) = \sum_{\nu\nu'} P^{(1)}_{\nu\nu'}(\mathbf{x}, \mathbf{x}'|\omega),$$
$$(10)$$

with

$$P^{(1)}_{\nu\nu'}(\mathbf{x}, \mathbf{x}'|\omega) = \frac{n_F(\mathcal{E}_{\nu'}) - n_F(\mathcal{E}_\nu)}{\hbar(\omega + i\delta) + \mathcal{E}_{\nu'} - \mathcal{E}_\nu}$$
$$\times \Psi_\nu(\mathbf{x})\Psi_\nu^*(\mathbf{x}')\Psi_{\nu'}(\mathbf{x}')\Psi_{\nu'}^*(\mathbf{x}) \qquad (11)$$

is the irreducible RPA polarization function with $\delta \to 0^+$. Using the wave functions of the CQWW, given in Eq. (2) in Eq. (11), we obtain

$$P^{(1)}(\mathbf{x}, \mathbf{x}'|\omega) = \frac{1}{2\pi L_z} \sum_{m,n=-\infty}^{\infty} \sum_{l,l'=1}^{\infty} \sum_{q_z=-\infty}^{\infty} e^{in(\varphi-\varphi')} e^{iq_z(z-z')} P^{(1)}_{\substack{m+n\ m\\ l\ l'}}(q_z, \omega)\eta_{\substack{m+n\ m\\ l\ l'}}(r)\eta^*_{\substack{m+n\ m\\ l\ l'}}(r'),$$
$$(12)$$

with

$$\eta_{\substack{m+n\ m\\ l\ l'}}(r) = \kappa_{m+n\,l}(r)\kappa^*_{ml'}(r)$$
$$(13)$$

and $n \equiv \Delta m = m' - m$. The RPA matrix polarization function $P^{(1)}_{\substack{m+n\ m\\ l\ l'}}(q_z, \omega)$ of the Q1DEG confined in a CQWW is

$$P^{(1)}_{\substack{m+n\ m\\ l\ l'}}(q_z, \omega) = \frac{1}{\pi L_z} \sum_{k_z=-\infty}^{\infty} \frac{n_F[\mathcal{E}_{ml'}(k_z)] - n_F[\mathcal{E}_{m+n\,l}(k_z + q_z)]}{\hbar(\omega + i\delta) + \mathcal{E}_{ml'}(k_z) - \mathcal{E}_{m+n\,l}(k_z + q_z)},$$
$$(14)$$

which gives at $T = 0$ K

$$\mathrm{Re}P^{(1)}_{\substack{m+n\ m\\ l\ l'}}(q_z, \omega) = -\frac{m_e}{2\pi^2\hbar^2 q_z}\left[\ln\left|\frac{k_F^{ml'} + q_z/2 - (m_e/\hbar q_z)(\omega - \Omega_{\substack{m+n\ m\\ l\ l'}})}{k_F^{ml'} - q_z/2 + (m_e/\hbar q_z)(\omega - \Omega_{\substack{m+n\ m\\ l\ l'}})}\right|\right.$$
$$\left. + \ln\left|\frac{k_F^{m+n\,l} + q_z/2 + (m_e/\hbar q_z)(\omega - \Omega_{\substack{m+n\ m\\ l\ l'}})}{k_F^{m+n\,l} - q_z/2 - (m_e/\hbar q_z)(\omega - \Omega_{\substack{m+n\ m\\ l\ l'}})}\right|\right]$$
$$(15)$$

and

$$\mathrm{Im}P^{(1)}_{\substack{m+n\ m\\ l\ l'}}(q_z, \omega) = -\frac{m_e}{2\pi\hbar^2|q_z|}\left\{\Theta\left[k_F^{ml'} + \frac{q_z}{2} - \frac{m_e}{\hbar q_z}(\omega - \Omega_{\substack{m+n\ m\\ l\ l'}})\right]\Theta\left[k_F^{ml'} - \frac{q_z}{2} + \frac{m_e}{\hbar q_z}(\omega - \Omega_{\substack{m+n\ m\\ l\ l'}})\right]\right.$$
$$\left. - \Theta\left[k_F^{m+n\,l} + \frac{q_z}{2} + \frac{m_e}{\hbar q_z}(\omega - \Omega_{\substack{m+n\ m\\ l\ l'}})\right]\Theta\left[k_F^{m+n\,l} - \frac{q_z}{2} - \frac{m_e}{\hbar q_z}(\omega - \Omega_{\substack{m+n\ m\\ l\ l'}})\right]\right\},$$
$$(16)$$

where the Fermi wave vector of subband $\{ml\}$ is $k_F^{ml} = [2m_e(E_F - \mathcal{E}_{ml})/\hbar^2]^{1/2}$ if for the Fermi energy $E_F > \mathcal{E}_{ml}$ is valid and zero for $E_F \le \mathcal{E}_{ml}$. $\Omega_{\substack{m\ m'\\ l\ l'}} = (\mathcal{E}_{ml} - \mathcal{E}_{m'l'})/\hbar$ is the subband separation frequency.

In the RPA and neglecting retardation effects the induced potential is related to the induced density by Poisson's equation, which reads for a CQWW

$$[\nabla_{\mathbf{x}_\perp} \cdot \varepsilon_s(\mathbf{x}_\perp)\nabla_{\mathbf{x}_\perp} - \varepsilon_s(\mathbf{x}_\perp) q_z^2]\phi^{\mathrm{ind}}(\mathbf{x}_\perp; q_z|\omega)$$
$$= -\frac{1}{\varepsilon_o}\rho^{\mathrm{ind}}(\mathbf{x}_\perp; q_z|\omega). \qquad (17)$$

Herein, ϕ^{ind} is the induced scalar potential, and $V^{\mathrm{ind}} = -e\phi^{\mathrm{ind}}$ is valid for an electron in the presence of ϕ^{ind}. Further, $\rho^{\mathrm{ind}} = -en_{\mathrm{ind}}$ is the induced electron charge

density, ε_o is the permittivity of vacuum, $\varepsilon_s(\mathbf{x}_\perp)$ is the static dielectric function of the semiconductor background arising from the high-energy electronic excitations across the band gap and the optical phonons, and $\mathbf{x}_\perp = (x, y)$. This is true because the frequencies of the optical phonons are usually larger than those of the Q1D plasmons.[15] $\varepsilon_s(\mathbf{x}_\perp)$ is a constant in each semiconductor: $\varepsilon_s(\mathbf{x}_\perp) = \varepsilon_{s1}$ for $r \leq R$, and $\varepsilon_s(\mathbf{x}_\perp) = \varepsilon_{s2}$ for $r > R$. Poisson's equation is solved by standard methods. Here we use the Green's function $D(\mathbf{x}, \mathbf{x}')$. This Green's function describes the electrostatic problem for the nonmagnetic background semiconductor without the Q1DEG. For inhomogeneous systems in which the materials have different but piecewise constant polarizabilities, the Green's function of Poisson's equation contains two parts, the direct Coulomb part, D^{dir}, and the image part, D^{im}. With the help of the Green's function the self-consistent potential is given by the following integral equation:

$$
\begin{aligned}
V^{\text{SC}}(\mathbf{x}_\perp; q_z|\omega) &= V^{\text{ext}}(\mathbf{x}_\perp; q_z|\omega) \\
&+ \frac{e^2}{\varepsilon_o} \int d^2 x'_\perp \int d^2 x''_\perp D(\mathbf{x}_\perp, \mathbf{x}'_\perp; \mathbf{q_z}) \\
&\times P^{(1)}(\mathbf{x}'_\perp, \mathbf{x}''_\perp; q_z|\omega) V^{\text{SC}}(\mathbf{x}''_\perp; q_z|\omega).
\end{aligned}
\tag{18}
$$

Performing matrix elements of this equation with the wave functions of Eq. (2) and assuming that collective excitations of the Q1DEG exist under the condition that $V^{\text{SC}} \neq 0$ while $V^{\text{ext}} = 0$, the existence conditions for collective excitations read

$$
\sum_{m=-\infty}^{\infty} \sum_{l,l'=1}^{\infty} [\delta_{m\, m_1-n} \delta_{l l_1} \delta_{l' l_2} - V^s_{\substack{m_1\, m_1-n\, m\, m+n \\ l_1\quad l_2\quad l'\quad l}}(q_z) \\
\times P^{(1)}_{\substack{m+n\, m \\ l\quad l'}}(q_z, \omega)] V^{\text{SC}}_{\substack{m+n\, m \\ l\quad l'}}(q_z, \omega) = 0. \tag{19}
$$

Herein $V^s_{\substack{m_1\, m_2\, m_3\, m_4 \\ l_1\quad l_2\quad l_3\quad l_4}}(q_z)$ is the matrix element of the Coulomb potential

$$
\begin{aligned}
V^s_{\substack{m_1\, m_2\, m_3\, m_4 \\ l_1\quad l_2\quad l_3\quad l_4}}(q_z) &= \frac{e^2}{\varepsilon_o} \Bigg[\int_0^R dr\, r \int_0^R dr'\, r' \eta^*_{\substack{m_1\, m_2 \\ l_1\quad l_2}}(r) \\
&\times D_n(r, r'; q_z)(r') \\
&\times \eta^*_{\substack{m_3\, m_4 \\ l_3\quad l_4}}(r') \Bigg] \\
&\times \delta_{m_2\, m_1-n} \delta_{m_4\, m_3+n}, \quad (20)
\end{aligned}
$$

where $D_n(r, r'; q_z) = D_n^{\text{dir}}(r, r'; q_z) + D_n^{\text{im}}(r, r'; q_z)$ with

$$
D_n^{\text{dir}}(r, r'; q_z) = \frac{1}{\varepsilon_{s1}} I_n(|q_z| r_<) K_n(|q_z| r_>), \tag{21}
$$

and

$$
D_n^{\text{im}}(r, r'; q_z) = \begin{cases} B_n\, I_n(|q_z| r) & \text{if } r \leq R \\ A_n\, K_n(|q_z| r) & \text{if } r > R. \end{cases} \tag{22}
$$

$I_n(x)$ and $K_n(x)$ are modified Bessel functions, $r_< = \min(r, r')$ and $r_> = \max(r, r')$, and the constants A_n and B_n are determined by the radial boundary conditions. The conditions $m_2 = m_1 - n$ and $m_4 = m_3 + n$ follow from the axial symmetry of the cylindrical potential. Further, we have defined

$$
V^{\text{SC}}_{\substack{m_1\, m_2 \\ l_1\quad l_2}}(q_z, \omega) = \left[\int_0^R dr\, r\, \eta^*_{\substack{m_1\, m_2 \\ l_1\quad l_2}} V_n^{\text{SC}}(r, q_z|\omega) \right] \\
\times \delta_{m_1\, m_2+n}, \quad (23)
$$

where $V_n^{\text{SC}}(r, q_z|\omega)$ is the Fourier transform of the screened potential $V^{\text{SC}}(\mathbf{x}, \omega)$. The system of Eqs. (19) is identical for $n \geq 0$ and $n \leq 0$. In the following we therefore restrict ourselves to the case $n \geq 0$ without loss of generality. According to the symmetry of the Green's function and the polarization function and the reality of the radial wave functions, the dispersion relation of the collective excitations of the Q1DEG in the CQWW, determining the intrasubband and intersubband plasmons, follows from Eq. (19), under the condition that this system of algebraic equations has nontrivial solution $V^{\text{SC}}_{\substack{m_1\, m_2 \\ l_1\quad l_2}}(q_z, \omega)$. The dispersion relation is given by

$$
\det[\delta_{m\, m_1-n} \delta_{l l_1} \delta_{l' l_2} - V^s_{\substack{m_1\, m_1-n\, m\, m+n \\ l_1\quad l_2\quad l'\quad l}}(q_z) \\
\times \chi^{(1)}_{\substack{m+n\, m \\ l\quad l'}}(q_z, \omega)] = 0. \quad (24)
$$

This equation determines the eigenfrequencies of the Q1D plasmons and each branch we denote by $\omega_p^{n,j}(q_z)$; $n \equiv \Delta m = 0, 1, 2, \ldots$ and $j = 1, 2, 3 \ldots$ numerates the modes for each n. The Q1D plasmons are connected with electron transitions $\{ml\} \to \{m'l'\}$. If this collective electron motion is within one subband the resulting mode is called intrasubband plasmon. In the case where this mode is connected with the collective electron transition between two different subbands this mode is called intersubband plasmon. Only under the condition that the different transitions are independent is each plasmon mode connected with one transition $\{ml\} \to \{m'l'\}$ and hence the plasmon dispersion curves are denoted by $\omega_p^{\substack{m'\, m \\ l'\quad l}}$. For the Q1D plasmons confined in CQWW's this is not true. Assuming that only the lowest subband is occupied the transitions with $n = 0$: $\{01\} \to \{01\}$, $\{01\} \to \{02\}$, $\{01\} \to \{03\}$, $\ldots$ are coupled but independent from $n = 1$: $\{01\} \to \{11\}$, $\{01\} \to \{12\}$, $\{01\} \to \{13\}$, $\ldots$ and $n = 2, 3, 4, 5, \ldots$. Hence the Q1D plasmon modes represent mixed states, i.e., are connected for each n with the above mentioned transitions. The resulting different branches for each n we numerate by j: $\omega_p^{n,j}(q_z)$. In Eq. (24) $\chi^{(1)}_{\substack{m+n\, m \\ l\quad l'}}(q_z, \omega)$ is the matrix polarization function given by

$$
\chi^{(1)}_{\substack{m+n\, m \\ l\quad l'}}(q_z, \omega) = \begin{cases} P^{(1)}_{\substack{m+n\, m \\ l\quad l'}}(q_z, \omega) + P^{(1)}_{\substack{m\, m+n \\ l'\quad l}}(q_z, \omega) & \text{if } m \neq -\left[\frac{n}{2}\right] \\ P^{(1)}_{\substack{\frac{n}{2}\, \frac{n}{2} \\ l\quad l'}}(q_z, \omega) & \text{if } m = -\frac{n}{2} \end{cases} \tag{25}
$$

where $\left[\frac{n}{2}\right]$ signifies the integral part of $\frac{n}{2}$. The matrix polarization function $\chi^{(1)}_{\underset{l}{m}\,\underset{l'}{m'}}(q_z,\omega)$ contains two physically different contributions: (i) the intrasubband contribution for $m = m'$ and $l = l'$ arising from electron excitations above the Fermi surface within one occupied subband and (ii) the intersubband contribution for $m \neq m'$ and $l \neq l'$, or $m \neq m'$ and $l = l'$, or $m = m'$ and $l \neq l'$ arising from electron excitations above the Fermi surface between two different subbands.

IV. COLLECTIVE EXCITATIONS: TWO SUBBANDS ARE OCCUPIED

To solve the complicated algebraic equation which determines the dispersion relation of the collective excitations it is necessary to restrict the discussion to a finite number of subbands. Here, we use the two-subband model. Hence we consider only the subbands $\mathcal{E}_{01}(k_z)$ and $\mathcal{E}_{11}(k_z)$. Because within the two-subband model the radial quantum numbers l_1, l_2, l_3, l_4 remain always fixed at "1," we omit the radial quantum number for simplicity. The spatial symmetry of the CQWW guarantees that the dispersion relation splits into two separate ones. One describes the modes for $n = 0$ and follows from Eq. (24) in the form

$$[1 - V^s_{0000}(q_z)\chi^{(1)}_{00}(q_z,\omega)][1 - V^s_{1111}(q_z)\chi^{(1)}_{11}(q_z,\omega)]$$

$$- V^s_{1100}(q_z)V^s_{0011}(q_z)\chi^{(1)}_{00}(q_z,\omega)\chi^{(1)}_{11}(q_z,\omega) = 0. \quad (26)$$

The second equation follows for $n = 1$ from Eq. (24),

$$1 - V^s_{1010}(q_z)\chi^{(1)}_{10}(q_z,\omega) = 0. \quad (27)$$

Equation (26) describes the intrasubband plasmons and Eq. (27) describes the intersubband plasmons. The intrasubband plasmons are connected with collective electron motion within the subbands {01} and {11}. Only in the case where the nondiagonal matrix elements of the Coulomb potential in Eq. (26) would vanish does the electron motion in both subbands become independent. Under such conditions the collective electron motion within each subband is described by a plasmon mode ω^{mm}_p, $m = 0,1$. But for the Q1DEG confined in a CQWW the nondiagonal matrix elements of the Coulomb potential are nonzero and hence the electron motion in both subbands becomes coupled. The mixing of the both modes ω^{mm}_p results in a rearrangement of the spectrum with the result that the new intrasubband plasmon modes $\omega^{0,1}_p$ and $\omega^{0,2}_p$ occur, which are connected with the electron motion in both subbands.

Until now most experiments on QWW's are done for the system GaAs-Ga$_{1-x}$Al$_x$As and the metal-oxide-semiconductor (MOS) system on InSb. The material constants used in the numerical calculations are, for GaAs, $\varepsilon_{s1} = 12.87$ and $m_e = 0.066\,24m_0$ (m_0: bare elecron mass) and for AlAs, $\varepsilon_{s2} = 10.22$. For InSb we use $\varepsilon_{s1} = 17.88$ and $m_e = 0.0139m_0$ and for SiO$_2$ $\varepsilon_{s2} = 3.8$.

A. Intrasubband plasmons

The dispersion relation of the intrasubband plasmons of the CQWW is Eq. (26). The full RPA dispersion curves of the two-subband model with two populated subbands are plotted in Fig. 1(a) for the InSb-MOS CQWW and in Fig. 1(b) for the GaAs-AlAs CQWW including the image potential (solid lines) and neglecting the image potential (dashed lines). The shaded areas in the ω-q_z plane are the regions where the (0-0) and (1-1) single-particle intrasubband excitations exist. The continua have the boundaries $\omega^{mm}_1 = \frac{\hbar k^{m1}_F}{m_e}q_z + \frac{\hbar}{2m_e}q^2_z$ and $\omega^{mm}_2 = \left|-\frac{\hbar k^{m1}_F}{m_e}q_z + \frac{\hbar}{2m_e}q^2_z\right|$ where $m = 0,1$. In these regions $\mathrm{Im}\chi^{(1)}_{00}(q_z,\omega)$ and $\mathrm{Im}\chi^{(1)}_{11}(q_z,\omega)$ are nonzero, re-
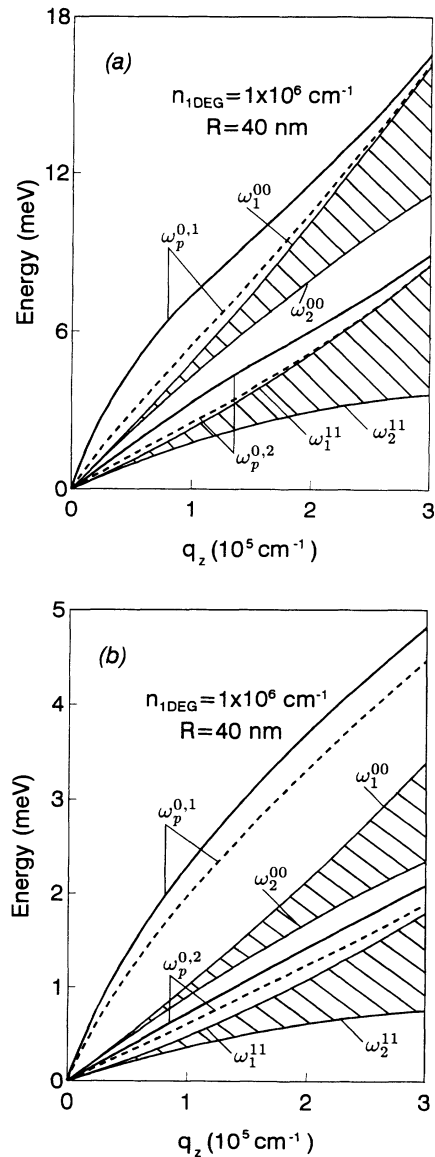
FIG. 1. Dispersion relation of the intrasubband plasmons of an InSb-MOS (a) and a GaAs-AlAs (b) CQWW where two subbands are occupied. The dispersion curves calculated including image effects are given by the solid lines and without image effects by the dashed lines. The shaded areas correspond to the single-particle intrasubband continua.

spectively, and hence the collective excitations become Landau damped. The dispersion curves of the intrasubband branches $\omega_p^{0,1}$ and $\omega_p^{0,2}$ start at $q_z = 0$ and $\omega = 0$ and approach for large wave vectors the boundaries ω_1^{11} and ω_1^{00}, respectively, of the single-particle intrasubband continua. Both intrasubband plasmon branches, $\omega_p^{0,1}$ and $\omega_p^{0,2}$, are connected with electron motion within both the lowest and first excited subband. The gap region between the boundaries ω_2^{00} and ω_1^{11} is free of Landau damping. Inside of this region the intrasubband plasmon branch $\omega_p^{0,2}$ exists. But we note that the branch $\omega_p^{0,2}$ only exists if the second subband $\mathcal{E}_{11}$ is occupied. The image forces exert a stronger influence on the intrasubband plasmons in InSb-MOS CQWW's than in GaAs-AlAs CQWW's for smaller wave vectors, but this becomes opposite for larger wave vectors (see also Fig. 2). The same behavior is also true for the upper plasmon branch and the lower plasmon branch, i.e., the upper plasmon branch is more strongly influenced by the image forces than the lower plasmon branch for smaller wave vectors and the opposite is true for larger wave vectors. The contribution of the image forces on the upper and lower branches is

26% and 23% at $q_z = 1 \times 10^5 \, \mathrm{cm}^{-1}$ and 2% and 4% at $q_z = 3 \times 10^5 \, \mathrm{cm}^{-1}$ for the InSb-MOS CQWW. The corresponding values for GaAs-AlAs system are 14%, 15% and 7%, 10%, respectively.

To get a deeper insight into the physical properties of both branches it is necessary to derive analytical expressions. In the small wave vector limit, i.e., $|q_z|/2 \ll k_F^{m1} - m_e\omega/\hbar|q_z| < k_F^{m1} + m_e\omega/\hbar|q_z|$, it follows for the matrix polarization function $(m = 0, 1)$ that

$$
P_{mm}^{(1)}(q_z, \omega) = \frac{m_e}{\pi^2 \hbar^2} \frac{k_F^{m1}}{[(m_e\omega/\hbar q_z)^2 - (k_F^{m1})^2]}
$$
$$
\times \left\{ 1 + \frac{[(k_F^{m1})^2 + 3(m_e\omega/\hbar q_z)^2] \, q_z^2}{12 \, [(k_F^{m1})^2 - (m_e\omega/\hbar q_z)^2]^2} \right.
$$
$$
\left. + O\left[\frac{1}{8} \left| k_F^{m1} - \frac{m_e\omega}{\hbar|q_z|} \right|^{-3} |q_z|^3 \right] \right\}. \tag{28}
$$

Using Eq. (28) for the matrix polarization functions and the Coulomb matrix elements in the small wave vector limit (Appendix) in Eq. (26) we obtain

$$
\omega_p^{\binom{0,1}{0,2}} = |q_z|R \left\{ \frac{1}{2R^2}[(v_F^{01})^2 + (v_F^{11})^2] + \frac{\omega_{s2}^2}{2}[-\ln(|q_z|R)] \right.
$$

$$
\left. \pm \left[\frac{1}{4R^4}[(v_F^{01})^2 - (v_F^{11})^2]^2 + \frac{\omega_{s2}^2}{2R^2} \frac{v_F^{01} - 2v_F^{11}}{v_F^{01} + 2v_F^{11}}[(v_F^{01})^2 - (v_F^{11})^2][-\ln(|q_z|R)] + \frac{\omega_{s2}^4}{4}[\ln(|q_z|R)]^2 \right]^{1/2} \right\}^{1/2}.
$$

$$
\tag{29}
$$

For $|q_z|R \to 0$, Eq. (29) reads

$$
\omega_p^{0,1} = \omega_{s2}|q_z|R \left[-\ln(|q_z|R) \right]^{1/2} \tag{30}
$$

and

$$
\omega_p^{0,2} = \left[v_F^{01} v_F^{11} \frac{2v_F^{01} + v_F^{11}}{2v_F^{11} + v_F^{01}} \right]^{1/2} |q_z|, \tag{31}
$$

with $\omega_{s2} = [n_{1\mathrm{DEG}}e^2/(2\pi\varepsilon_o\varepsilon_{s2}m_eR^2)]^{1/2}$ and $v_F^{m1} = \hbar k_F^{m1}/m_e$ the Fermi velocity in subband $\{m1\}$. The branch $\omega_p^{0,2}$ has in lowest order of $|q_z|R$ a linear dispersion and depends only on the carrier density and not on the dielectric screening.

The quotients of the eigenfrequencies of the intrasubband plasmon branches including the image potential $(\omega_p^{0,j})$ and neglecting the image potential $(\omega_{p_{\mathrm{dir}}}^{0,j})$ are plotted in Fig. 2. It is seen that the influence of the image forces on the plasmon branch $\omega_p^{0,1}$ decreases monotonically from $\omega_p^{0,1}/\omega_{p_{\mathrm{dir}}}^{0,1} = 4.7$ for $|q_z|R = 0$ and vanishes $(\omega_p^{0,1}/\omega_{p_{\mathrm{dir}}}^{0,1} = 1)$ for $|q_z|R \to \infty$. The physical reason for this behavior is that in the limit of large $|q_z|R$ nearly all field lines of the Coulomb potential are inside of the CQWW. On the other hand, in the limit $|q_z|R \to 0$ nearly all field lines are outside of the CQWW, but inside the surrounding medium and so the image effect

FIG. 2. The ratio of the dispersion relations of the upper $\omega_p^{0,1}$ and lower $\omega_p^{0,2}$ intrasubband plasmon branches including the image potential with the dispersion relation $\omega_{p_{\mathrm{dir}}}^{0,1}$ and $\omega_{p_{\mathrm{dir}}}^{0,2}$, respectively, calculated neglecting the image potential. The solid lines correspond to the InSb-MOS CQWW and the dashed lines to the GaAs-AlAs CQWW.

reaches its maximum value. For the intrasubband plasmon branch $\omega_p^{0,2}$ the image forces have vanishing influence for $|q_z|R \to 0$ and $|q_z|R \to \infty$. The vanishing influence of the image effect for $|q_z|R \to 0$ is the result of the fact that the branch $\omega_p^{0,2}$ behaves like an acoustic plasmon (see Sec. V). The induced charge density of this excitation vanishes in this limit and thus the image effect vanishes too. Further, it is seen that the image effects more strongly influence the Q1D intrasubband modes of the InSb-MOS CQWW for smaller wave vectors ($q_z R < 0.8$) but for larger wave vectors the Q1D plasmon modes of the GaAs-AlAs CQWW are more strongly influenced. In the case of large wave vectors the lower frequency plasmon branch $\omega_p^{0,2}$ is more strongly influenced by the image forces than the upper ones $\omega_p^{0,1}$.

B. Intersubband plasmons

The dispersion relation of the Q1D intersubband plasmons of the two-subband model, assuming that two subbands are occupied, is given by Eq. (27). In Fig. 3 the full RPA dispersion curves of the two-subband model with two populated subbands are plotted including the image potential (solid lines) and neglecting the image contribution (dashed lines) for the InSb-MOS CQWW [Fig. 3(a)] and for the GaAs-AlAs CQWW [Fig. 3(b)]. The shaded area in the ω-q_z plane is the single-particle intersubband continuum $[\mathrm{Im}\chi_{10}^{(1)}(q_z,\omega) \neq 0]$ which has the boundaries $\omega_1^{10} = \frac{\hbar k_F^{01}}{m_e}q_z + \frac{\hbar}{2m_e}q_z^2 + \Omega_{10}$, $\omega_2^{10} = \left|-\frac{\hbar k_F^{01}}{m_e}q_z + \frac{\hbar}{2m_e}q_z^2 + \Omega_{10}\right|$, $\omega_3^{10} = \left|\frac{\hbar k_F^{11}}{m_e}q_z - \frac{\hbar}{2m_e}q_z^2 + \Omega_{10}\right|$, $\omega_4^{10} = \left|-\frac{\hbar k_F^{11}}{m_e}q_z - \frac{\hbar}{2m_e}q_z^2 + \Omega_{10}\right|$. If two subbands are occupied, a gap region, the area between the curves ω_3^{10} and ω_4^{10}, arises, for which $\mathrm{Im}\chi_{10}^{(1)} = 0$. Within this region the additional intersubband plasmon mode $\omega_p^{1,2}$ exists. This additional branch of an intersubband plasmon was predicted by Wendler et al.[15] and Mendoza and Schaich.[13] It is seen from Fig. 3 that the fundamental mode $\omega_p^{1,1}$ has a finite depolarization shift and a positive dispersion, the additional mode $\omega_p^{1,2}$ has a vanishing depolarization shift at $q_z = 0$ and a negative dispersion.

The quotients of the eigenfrequencies of the intersubband plasmon branches including image effects $(\omega_p^{1,j})$ and neglecting image effects $(\omega_{p_{\mathrm{dir}}}^{1,j})$ are plotted in Fig. 4. It is clearly seen that the influence of the image forces for
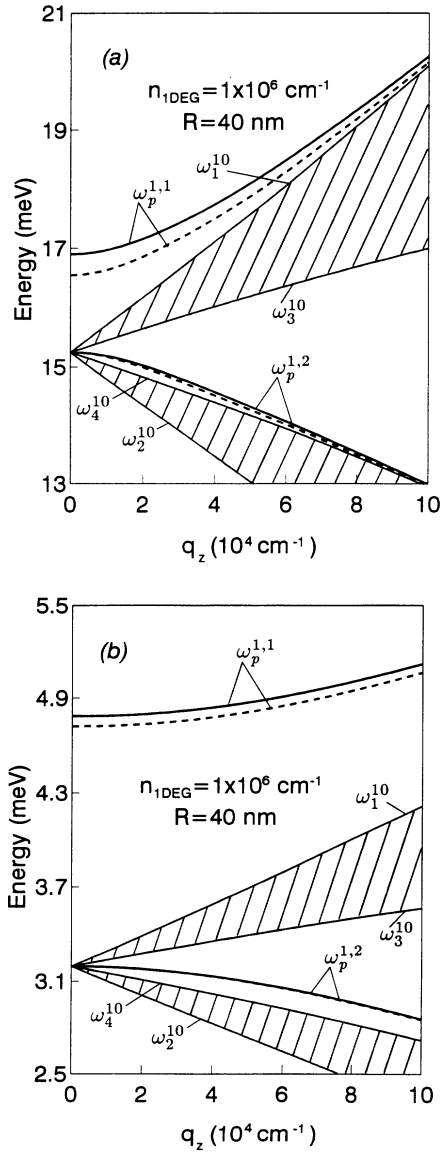
FIG. 3. Dispersion relation of the intersubband plasmons of an InSb-MOS (a) and a GaAs-AlAs (b) CQWW where two subbands are occupied. The dispersion curves calculated including image effects are given by the solid lines and without image effects by the dashed lines. The shaded areas correspond to the single-particle intrasubband continua.
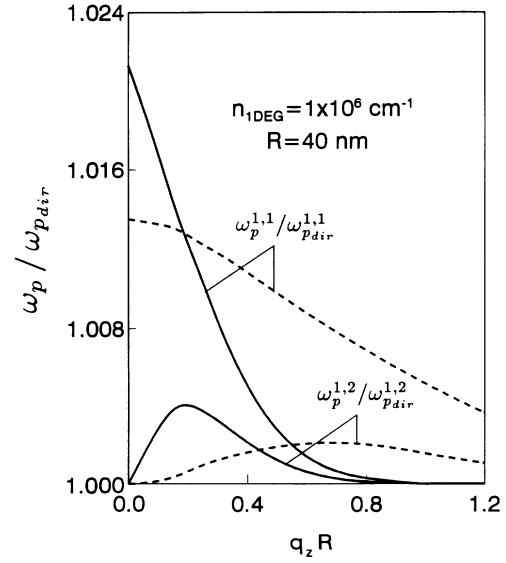
FIG. 4. The ratio of the dispersion relations of the upper $\omega_p^{1,1}$ and lower $\omega_p^{1,2}$ intersubband plasmon branches including the image potential with the dispersion relations $\omega_{p_{\mathrm{dir}}}^{1,1}$ and $\omega_{p_{\mathrm{dir}}}^{1,2}$, respectively, calculated neglecting the image potential. The solid lines correspond to the InSb-MOS CQWW and the dashed lines to the GaAs-AlAs CQWW.

$\omega_p^{1,1}$ decreases monotonically with increasing wave vector q_z and vanishes in the limit $|q_z|R \to \infty$. For the intersubband plasmon branch $\omega_p^{1,2}$ the image forces have vanishing influence for $|q_z|R \to 0$ and $|q_z|R \to \infty$. If we compare Fig. 2 with Fig. 4 we see that the plasmon branches $\omega_p^{0,1}$ and $\omega_p^{1,1}$ on the one side and $\omega_p^{0,2}$ and $\omega_p^{1,2}$ on the other side show a similar dependence on the image forces over the wave vector because of the same physical

reasons as described above. In general, the influence of the image forces on the Q1D intrasubband plasmons is stronger than on the intersubband plasmon.

To get a deeper insight into the physical properties of both modes we derive analytical expressions in the limit of small wave vectors. In this limit, i.e., $v_F^{01}|q_z|, \hbar q_z^2/2m_e \ll \omega - \Omega_{10}$, the needed matrix polarization function reads

$$P_{\binom{10}{01}}^{(1)}(q_z,\omega) = -\frac{m_e}{2\pi^2\hbar^2 q_z}\left\{\pm\frac{\hbar\pi q_z(n_{1\mathrm{DEG}}^{01} - n_{1\mathrm{DEG}}^{11})}{m_e(\omega \pm \Omega_{10})} - \frac{\hbar^2\pi q_z^3 n_{1\mathrm{DEG}}}{2m_e^2(\omega \pm \Omega_{10})^2} + O\left[\left|\frac{\hbar q_z}{m_e}\left(\frac{k_F^{01} + |q_z|/2}{\omega \pm \Omega_{10}}\right)\right|^3\right]\right\}, \tag{32}$$

where $n_{1\mathrm{DEG}} = \sum_m \sum_l n_{1\mathrm{DEG}}^{ml}$ with $n_{1\mathrm{DEG}}^{ml} = \frac{4}{\pi\hbar}\sqrt{\frac{m_e}{2}}\sqrt{E_F - \mathcal{E}_{ml}}$ the 1D electron number density of the subband $\{ml\}$. Using this long-wavelength expression of $P_{\binom{10}{01}}^{(1)}(q_z,\omega)$ and the Coulomb matrix element $V_{1010}^s(q_z)$ (Appendix) in the dispersion relation, Eq. (27), we obtain

$$\omega_p^{1,1} \approx (1 + \alpha_{1,1})^{1/2}\Omega_{10}, \tag{33}$$

with

$$\alpha_{1,1} = \frac{(n_{1\mathrm{DEG}}^{01} - n_{1\mathrm{DEG}}^{11})e^2}{\pi\varepsilon_o\varepsilon_{s1}\hbar\Omega_{10}}\left(\frac{2}{7} + \frac{1}{8}\frac{\varepsilon_{s1} - \varepsilon_{s2}}{\varepsilon_{s1} + \varepsilon_{s2}}\right). \tag{34}$$

As seen from Eq. (33), the image contribution enters the zero-order term of the intersubband plasmon branch $\omega_p^{1,1}$. This behavior is different from the case of intersubband plasmons of a quasi-two-dimensional electron gas, where the image contribution enters the first-order term of an expansion in powers of the wave vector (see, for instance, Ref. 38). It is seen from Eq. (34) that the image contribution to the depolarization shift is independent from the diameter of the wire. The maximum contribution of the image forces to the depolarization shift is 17%. In the leading order of $|q_z|R$ and if $v_F^{m1}|q_z| \gg \hbar q_z^2/2m_e$, $|\omega - \Omega_{10}|$ we obtain

$$\omega_p^{1,2} \approx \Omega_{10} - \xi q_z^2, \tag{35}$$

with

$$\xi = \frac{\pi^2\hbar^2}{m_e V_{1010}^s(0)}\frac{v_F^{01}v_F^{11}}{v_F^{01} - v_F^{11}} + \frac{\hbar}{2m_e}\frac{v_F^{01} + v_F^{11}}{v_F^{01} - v_F^{11}} + \frac{v_F^{01}v_F^{11}}{2\Omega_{10}}. \tag{36}$$

Because of $v_F^{01} > v_F^{11}$ it follows that for all electron densities $\xi > 0$ is valid. Hence the explicit analytical expression of $\omega_p^{1,2}$, Eq. (35), shows the negative dispersion.

V. INDUCED DENSITY OF THE COLLECTIVE EXCITATIONS

In the previous sections, we have calculated the eigenfrequencies of the Q1D plasmons of a CQWW which have the branches $\omega_p^{0,1}$, $\omega_p^{0,2}$, $\omega_p^{1,1}$, and $\omega_p^{1,2}$ for a two-subband model with two occupied subbands. The plasmon branches $\omega_p^{0,2}$ and $\omega_p^{1,2}$ only occur if the second sub-

band is occupied whereas the plasmon branches $\omega_p^{0,1}$ and $\omega_p^{1,1}$ exist also if only one subband is occupied. In this section we want to investigate the physical nature of the different branches in detail.

The induced electron number density $n_{\mathrm{ind}}(\mathbf{x},t)$ is given by

$$n_{\mathrm{ind}}(\mathbf{x},t) = \frac{1}{2\pi}\int_{-\infty}^{\infty}d\omega\, e^{-i\omega t}\, n_{\mathrm{ind}}(\mathbf{x},\omega), \tag{37}$$

where $n_{\mathrm{ind}}(\mathbf{x},\omega)$ is given by Eq. (9). Using the wave functions of the CQWW, Eq. (2), in Eqs. (9) and (37) we obtain

$$n_{\mathrm{ind}}(\mathbf{x},t) = \sum_{n=0}^{\infty}\sum_{q_z=0}^{\infty}\int_0^{\infty}d\omega\, n_{\mathrm{ind}}^{(n)}(\mathbf{x},t|q_z,\omega), \tag{38}$$

with

$$n_{\mathrm{ind}}^{(n)}(\mathbf{x},t|q_z,\omega) = \frac{1}{(2\pi)^2 L_z}e^{i(n\varphi + q_z z - \omega t)}$$

$$\times \sum_{m=-\infty}^{\infty}\sum_{l,l'=1}^{\infty}\eta_{\substack{m+n\ m\\l'\ l}}(r)P_{\substack{m+n\ m\\l'\ l}}^{(1)}(q_z,\omega)$$

$$\times V_{\substack{m+n\ m\\l'\ l}}^{\mathrm{SC}}(q_z,\omega) + \mathrm{c.c.}$$

$$= \sum_{m=-\infty}^{\infty}\sum_{l=1}^{\infty}n_{\mathrm{ind}}^{(n;m,l)}(\mathbf{x},t|q_z,\omega), \tag{39}$$

where c.c. means complex conjugated. In Eq. (39) $n_{\mathrm{ind}}^{(n)}(\mathbf{x},t|q_z,\omega)$ is the electron number density at $(\mathbf{x},t)$ induced if the Q1DEG oscillates with ω. Hence $n_{\mathrm{ind}}^{(n;m,l)}(\mathbf{x},t|q_z,\omega_p^{n,j})$ is the induced electron number density at $(\mathbf{x},t)$ induced in subband $\{ml\}$, if the Q1DEG oscillates in the plasmon mode with the dispersion relation $\omega_p^{n,j}(q_z)$.

A. Intrasubband plasmons

We want to consider the intrasubband plasmon branches $(n = 0;\ m = 0,\pm 1;\ l,l' = 1)$. In this case we have

$$n_{\mathrm{ind}}^{(0;0,1)}(\mathbf{x},t|q_z,\omega) = \frac{1}{(2\pi)^2 L_z}e^{i(q_z z - \omega t)}$$

$$\times [\eta_{00}(r)P_{00}^{(1)}(q_z,\omega)$$

$$\times V_{00}^{\mathrm{SC}}(q_z,\omega)] + \mathrm{c.c.} \tag{40}$$

and

$$n_{\text{ind}}^{(0;1,1)}(\mathbf{x},t|q_z,\omega) = \frac{1}{(2\pi)^2 L_z}e^{i(q_z z-\omega t)}$$
$$\times[\eta_{11}(r)P_{11}^{(1)}(q_z,\omega)V_{11}^{\text{SC}}(q_z,\omega)]$$
$$+\text{c.c.}, \qquad (41)$$

where $n_{\text{ind}}^{(0;1,1)}(\mathbf{x},t|q_z,\omega) = n_{\text{ind}}^{(0;-1,1)}(\mathbf{x},t|q_z,\omega)$ is valid and we drop $l = l' = 1$ for simplicity. Because $V_{0000}^s(q_z) = V_{1111}^s(q_z) = V_{1100}^s(q_z) = V_{0011}^s(q_z) \approx -e^2/(\varepsilon_o\varepsilon_{s2})\ln(|q_z|R)$ in the lowest order of $|q_z|R$ we obtain from Eq. (19)

$$P_{11}^{(1)}(q_z,\omega)V_{11}^{\text{SC}}(q_z,\omega)$$

$$= \frac{1-V_{0000}^s(q_z)P_{00}^{(1)}(q_z,\omega)}{2V_{0000}^s(q_z)}V_{00}^{\text{SC}}(q_z,\omega). \qquad (42)$$

For the discussion of the induced electron number density of the two intrasubband plasmon branches $\omega_p^{0,1}$ and $\omega_p^{0,2}$ we use the lowest-order expressions of $P_{00}^{(1)}(q_z,\omega)$, Eq. (28), and the explicit dispersion relations, Eqs. (30) and (31). For the upper branch $\omega_p^{0,1}$ it follows that

$$P_{00}^{(1)}(q_z,\omega_p^{0,1}) \approx -\frac{2\varepsilon_0\varepsilon_{s2}k_F^{01}}{\pi n_{\text{1DEG}}e^2\ln(|q_z|R)} > 0 \qquad (43)$$

and

$$\frac{1-V_{0000}^s(q_z)P_{00}^{(1)}(q_z,\omega_p^{0,1})}{2V_{0000}^s(q_z)} \approx -\frac{\varepsilon_0\varepsilon_{s2}k_F^{11}}{\pi n_{\text{1DEG}}e^2\ln(|q_z|R)} > 0. \qquad (44)$$

Hence the induced electron number densities in subband $m = 0$ and subband $m = \pm 1$ oscillate in phase if the branch $\omega_p^{0,1}$ is excited and following that the upper branch $\omega_p^{0,1}$ behaves like an optical plasmon. For the lower branch $\omega_p^{0,2}$ it follows that

$$P_{00}^{(1)}(q_z,\omega_p^{0,2}) \approx \frac{m_e}{\pi^2\hbar^2}\frac{2k_F^{11}+k_F^{01}}{(k_F^{11})^2-(k_F^{01})^2} < 0 \qquad (45)$$

and

$$\frac{1-V_{0000}^s(q_z)P_{00}^{(1)}(q_z,\omega_p^{0,2})}{2V_{0000}^s(q_z)} \approx \frac{m_e}{2\pi^2\hbar^2}\frac{2k_F^{11}+k_F^{01}}{(k_F^{01})^2-(k_F^{11})^2} > 0. \qquad (46)$$

This indicates that the densities, induced in subband $m = 0$ and subband $m = 1$, oscillate in antiphase if the intrasubband plasmon branch $\omega_p^{0,2}$ is excited. Thus the lower intrasubband plasmon branch $\omega_p^{0,2}$ behaves like an acoustic plasmon.

Integrating $n_{\text{ind}}^{(0)}(\mathbf{x},t|q_z,\omega) = n_{\text{ind}}^{(0;0,1)}(\mathbf{x},t|q_z,\omega) + 2n_{\text{ind}}^{(0;1,1)}(\mathbf{x},t|q_z,\omega)$ over the cross section of the CQWW we obtain the number of induced electrons per unit length,

$$\int_0^{2\pi}d\varphi\int_0^R dr\, r\, n_{\text{ind}}^{(0)}(\mathbf{x},t|q_z,\omega) = \frac{1}{2\pi L_z}e^{i(q_z z-\omega t)}\left[P_{00}^{(1)}(q_z,\omega)+\frac{1-V_{0000}^s(q_z)P_{00}^{(1)}(q_z,\omega)}{V_{0000}^s(q_z)}\right]V_{00}^{\text{SC}}(q_z,\omega)+\text{c.c.} \qquad (47)$$

Using Eqs. (43) and (44) for the optical plasmon and (45) and (46) for the acoustic plasmon, Eq. (47) gives a nonzero value for the optical plasmon branch but a vanishing value for the acoustic plasmon branch in the limit $|q_z|R \to 0$. This different behavior of the induced electron density of both branches in the limit $|q_z|R \to 0$ results in the different influence of the image forces on both branches (see discussion in Sec. IV A) and this is the reason that $\omega_p^{0,1} > \omega_p^{0,2}$.

B. Intersubband plasmons

In Sec. IV B we have obtained two intersubband plasmon branches ($n = 1$; $m = 0,\pm 1$; $l,l' = 1$). In this case we have

$$n_{\text{ind}}^{(1;0,1)}(\mathbf{x},t|q_z,\omega) = \frac{1}{(2\pi)^2 L_z}e^{i(\varphi+q_z z-\omega t)}$$
$$\times[\eta_{10}(r)P_{10}^{(1)}(q_z,\omega)V_{10}^{\text{SC}}(q_z,\omega)] + \text{c.c.} \qquad (48)$$

and

$$n_{\text{ind}}^{(1;1,1)}(\mathbf{x},t|q_z,\omega) = \frac{1}{(2\pi)^2 L_z}e^{i(\varphi+q_z z-\omega t)}$$
$$\times[\eta_{01}(r)P_{01}^{(1)}(q_z,\omega)V_{01}^{\text{SC}}(q_z,\omega)]$$
$$+\text{c.c.}, \qquad (49)$$

where $V_{10}^{\text{SC}}(q_z,\omega) = V_{01}^{\text{SC}}(q_z,\omega)$ and $\eta_{10}(r) = \eta_{01}(r)$ are valid. For the discussion of the induced electron number density of the two intersubband plasmon branches $\omega_p^{1,1}$ and $\omega_p^{1,2}$ we use the lowest-order expressions of $P_{10}^{(1)}(q_z,\omega)$ and $P_{01}^{(1)}(q_z,\omega)$ given in Eq. (32), and the explicit dispersion relations, Eqs. (33) and (35). For the upper branch $\omega_p^{1,1}$ it follows that

$$P_{10}^{(1)}(q_z,\omega_p^{1,1}) \approx \frac{k_F^{01}-k_F^{11}}{\pi^2\hbar(\omega_p^{1,1}-\Omega_{10})} > 0 \qquad (50)$$

and

$$P_{01}^{(1)}(q_z,\omega_p^{1,1}) \approx \frac{k_F^{11}-k_F^{01}}{\pi^2\hbar(\omega_p^{1,1}+\Omega_{10})} < 0. \qquad (51)$$

Hence the induced electron number densities in subband $m = 0$ and subband $m = 1$ have different signs and

therefore oscillate in antiphase if the plasmon branch $\omega_p^{1,1}$ is excited. Note that $P_{10}^{(1)}(q_z, \omega_p^{1,2}) > |P_{01}^{(1)}(q_z, \omega_p^{1,2})|$ is valid. Thus the upper intersubband plasmon branch $\omega_p^{1,1}$ behaves like an acoustic plasmon.

If we look for the lower intersubband plasmon branch $\omega_p^{1,2}$ we can see that for $q_z \to 0$ and $\omega \to \Omega_{10}$ Eq. (14) diverges for $\delta \to +0$ and the analytical expressions for $P_{10}^{(1)}(q_z = 0, \omega = \Omega_{10})$, Eqs. (15) and (16), become indeterminate. From Eq. (48) it follows that we must have $V_{10}^{SC}(q_z = 0, \omega = \Omega_{10}) = 0$ to avoid unphysical divergencies of the induced electron number density. Poisson's equation, Eq. (17), gives then the result that for $q_z = 0$ and $\omega = \Omega_{10}$ the induced electron number density vanishes: $n_{ind}^{(1)}(\mathbf{x}, t | q_z = 0, \omega_p^{1,2} = \Omega_{10}) = 0$. Hence the depolarization shift must vanish too and in this limiting case there is no excitation. This is a result of the resonant screening, i.e., at the intersubband separation frequency Ω_{10} the electrons completely screen the external fields.

For the lower branch $\omega_p^{1,2}$ and for the small but nonzero q_z it follows that

$$P_{10}^{(1)}(q_z, \omega_p^{1,2}) \approx -\frac{m_e}{2\pi^2\hbar^2}$$
$$\times \left[\frac{1}{k_F^{01}} + \frac{1}{k_F^{11}} - \frac{2m_e\xi}{\hbar}\left(\frac{1}{k_F^{11}} - \frac{1}{k_F^{01}}\right)\right]$$
$$> 0 \tag{52}$$

and

$$P_{01}^{(1)}(q_z, \omega_p^{1,2}) \approx -\frac{k_F^{01} - k_F^{11}}{2\pi^2\hbar\Omega_{10}} < 0. \tag{53}$$

Hence in this case the induced electron number densities in subband $m = 0$ and subband $m = 1$ have different signs too and subsequently oscillate in antiphase if the intersubband plasmon branch $\omega_p^{1,2} \neq \Omega_{10}$ is excited. Thus the lower intersubband plasmon branch $\omega_p^{1,2}$ behaves like an acoustic plasmon. But in comparison with the upper plasmon branch $\omega_p^{1,1}$ the induced electron number density of the lower plasmon branch $\omega_p^{1,2}$ vanishes for $q_z \to 0$.

VI. CONCLUSION

In this paper we have studied the collective excitations of CQWW's within the full RPA for a two-subband model if two subbands are occupied. It is shown that there are two different modes, the intrasubband and intersubband plasmons, each split into two branches. The occurrence of the second branch is the result of the occupation of the second subband. The upper intrasubband plasmon branch behaves like an optical plasmon, i.e., the electron number densities induced in both subbands oscillate in phase. But the lower intrasubband plasmon branch is characterized by an electron number density oscillating in antiphase in both subbands and hence is an acoustic plasmon. If the Q1DEG of the CQWW oscillates in an intersubband plasmon branch, the induced electron number density of both subbands oscillates in antiphase and it follows that both branches have the character of acous-

tic plasmon. In the limit of the vanishing wave vectors the induced electron number density of the Q1DEG is nonzero when oscillating in the upper intersubband plasmon branch but tends to zero when oscillating in the lower intersubband plasmon mode.

The classification of the modes in optical and acoustic modes is well known in the physics of multicomponent plasmas. Recently, Bonitz et al.[39] investigated an electron-hole plasma, confined in a QWW and found optical and acoustic modes. Further, Shikin et al.[21] calculated within the Thomas-Fermi model the Q1D plasmons of two coupled QWW's. The resulting modes could be classified into optical and acoustic plasmons. But we note that in Ref. 21 the classification is according to the electron number density induced in both wires whereas in our calculations only one wire with two occupied subbands is considered. Hence we hope that the present results give a deeper insight into the physical properties of the Q1D plasmons of one isolated quantum-well wire. Especially, the nature of the additional modes which occur if more than one subband is occupied should become more clear.

Further, we have shown the importance of the inclusion of the image effects on the Coulomb interaction potential in a relatively wide range of the wave vector ($|q_z|R \approx 1$). The image forces increase the eigenfrequencies of the Q1D plasmons in GaAs-AlAs and InSb-MOS CQWW's. The influence of the image forces is stronger for the intrasubband plasmons than for the intersubband plasmons. It is shown that the two branches of intrasubband and intersubband plasmons have a different dependence on the image potential when varying the wave vector. The two plasmon branches $\omega_p^{0,1}$ and $\omega_p^{1,1}$, present also if one subband is occupied, show a monotonically decreasing image influence with increasing wave vector. The other two plasmon branches $\omega_p^{0,2}$ and $\omega_p^{1,2}$, only present if the second subband is occupied, show vanishing image influence for zero and infinite wave vectors.

APPENDIX: MATRIX ELEMENTS OF THE COULOMB POTENTIAL

In this appendix we calculate the small wave vector ($|q_z|R \ll 1$) expressions of the direct Coulomb potential and the image potential $V_{m_1m_2m_3m_4}^{im}(q_2)$ defined in Eqs. (18)-(20) using the wave function of Eqs. (6) and (7):

$$V_{m_1m_2m_3m_4}^{s}(q_z) = V_{m_1m_2m_3m_4}^{dir}(q_z) + V_{m_1m_2m_3m_4}^{im}(q_z).$$

The calculation is straightforward with the following results:

$$V_{0000}^{dir}(q_z) \approx -\frac{e^2}{\varepsilon_o\varepsilon_{s1}}\left\{\ln\left(\frac{\gamma|q_z|R}{2}\right) - 0.6083 + (q_zR)^2\left[\frac{1}{8}\ln\left(\frac{\gamma|q_z|R}{2}\right) - 0.1450\right]\right\}, \tag{A1}$$

$$V_{0000}^{\text{im}}(q_z) \approx \frac{e^2}{\varepsilon_o}\left(\frac{1}{\varepsilon_{s1}}-\frac{1}{\varepsilon_{s2}}\right)\left\{\ln\left(\frac{\gamma|q_z|R}{2}\right)+(q_zR)^2\left[\frac{\varepsilon_{s1}}{2\varepsilon_{s2}}\ln^2\left(\frac{\gamma|q_z|R}{2}\right)+\frac{1}{8}\ln\left(\frac{\gamma|q_z|R}{2}\right)-\frac{1}{4}\right]\right\}, \tag{A2}$$

$$V_{1100}^{\text{dir}}(q_z) \approx -\frac{e^2}{\varepsilon_o\varepsilon_{s1}}\left\{\ln\left(\frac{\gamma|q_z|R}{2}\right)-0.4476+(q_zR)^2\left[\frac{13}{80}\ln\left(\frac{\gamma|q_z|R}{2}\right)-0.1715\right]\right\}, \tag{A3}$$

$$V_{1100}^{\text{im}}(q_z) \approx \frac{e^2}{\varepsilon_o}\left(\frac{1}{\varepsilon_{s1}}-\frac{1}{\varepsilon_{s2}}\right)\left\{\ln\left(\frac{\gamma|q_z|R}{2}\right)+(q_zR)^2\left[\frac{\varepsilon_{s1}}{2\varepsilon_{s2}}\ln^2\left(\frac{\gamma|q_z|R}{2}\right)+\frac{13}{80}\ln\left(\frac{\gamma|q_z|R}{2}\right)-\frac{1}{4}\right]\right\}, \tag{A4}$$

$$V_{1111}^{\text{dir}}(q_z) \approx -\frac{e^2}{\varepsilon_o\varepsilon_{s1}}\left\{\ln\left(\frac{\gamma|q_z|R}{2}\right)-0.3673+(q_zR)^2\left[\frac{1}{5}\ln\left(\frac{\gamma|q_z|R}{2}\right)-0.0735\right]\right\}, \tag{A5}$$

$$V_{1111}^{\text{im}}(q_z) \approx \frac{e^2}{\varepsilon_o}\left(\frac{1}{\varepsilon_{s1}}-\frac{1}{\varepsilon_{s2}}\right)\left\{\ln\left(\frac{\gamma|q_z|R}{2}\right)+(q_zR)^2\left[\frac{\varepsilon_{s1}}{2\varepsilon_{s2}}\ln^2\left(\frac{\gamma|q_z|R}{2}\right)+\frac{1}{5}\ln\left(\frac{\gamma|q_z|R}{2}\right)-\frac{1}{4}\right]\right\}, \tag{A6}$$

$$V_{1010}^{\text{dir}}(q_z) \approx \frac{e^2}{\varepsilon_o\varepsilon_{s1}}\left\{\frac{2}{7}+(q_zR)^2\left[\frac{1}{16}\ln\left(\frac{\gamma|q_z|R}{2}\right)-0.0453\right]\right\}, \tag{A7}$$

$$V_{1010}^{\text{im}}(q_z) \approx \frac{e^2}{\varepsilon_o\varepsilon_{s1}}\frac{\varepsilon_{s1}-\varepsilon_{s2}}{\varepsilon_{s1}+\varepsilon_{s2}}\left(\frac{1}{8}+\frac{(q_zR)^2}{4}\left\{\frac{1}{16}\frac{\varepsilon_{s2}-\varepsilon_{s1}}{\varepsilon_{s2}+\varepsilon_{s1}}\left[1+4\ln\left(\frac{\gamma|q_z|R}{2}\right)\right]-\frac{1}{5}\right\}\right), \tag{A8}$$

where $\gamma = 1.781\,072\,418$ is the Euler constant.

[1] W. Hansen, M. Horst, J.P. Kotthaus, U. Merkt, Ch. Sikorski, and K. Ploog, Phys. Rev. Lett. **58**, 2586 (1987).

[2] F. Brinkop, W. Hansen, J.P. Kotthaus, and K. Ploog, Phys. Rev. B **37**, 6547 (1988).

[3] T. Demel, D. Heitmann, P. Grambow, and K. Ploog, Phys. Rev. Lett. **66**, 2657 (1991).

[4] H. Drexler, W. Hansen, J.P. Kotthaus, M. Holland, and S.P. Beaumont, Phys. Rev. B **46**, 12849 (1992).

[5] A.R. Goñi, A. Pinczuk, J.S. Weiner, J. M. Calleja, B.S. Dennis, L.N. Pfeiffer, and K.W. West, Phys. Rev. Lett. **67**, 3298 (1991).

[6] A.R. Goñi, A. Pinczuk, J.S. Weiner, B.S. Dennis, L.N. Pfeiffer, and K.W. West, Phys. Rev. Lett. **70**, 1151 (1993).

[7] S. Das Sarma and W.Y. Lai, Phys. Rev. B **32**, 1401 (1985).

[8] W. Que and G. Kirczenow, Phys. Rev. B **37**, 7153 (1988).

[9] A.V. Chaplik, Superlatt. Microstruct. **6**, 329 (1989).

[10] A. Gold and A. Ghazali, Phys. Rev. B **41**, 7626 (1990).

[11] F.Y. Huang, Phys. Rev. B **41**, 12957 (1990).

[12] W. Que, Phys. Rev. B **43**, 7127 (1991).

[13] B.S. Mendoza and W.L. Schaich, Phys. Rev. B **43**, 9275 (1991).

[14] Q.P. Li and S. Das Sarma, Phys. Rev. B **43**, 11768 (1991).

[15] L. Wendler, R. Haupt, and R. Pechstedt, Phys. Rev. B **43**, 14669 (1991).

[16] G.Y. Hu and R.F. O'Connell, Phys. Rev. B **44**, 3140 (1991).

[17] R. Haupt, L. Wendler, and R. Pechstedt, Phys. Rev. B **44**, 13635 (1991).

[18] L. Wendler, R. Haupt, and R. Pechstedt, Surf. Sci. **263**, 363 (1992).

[19] L. Wendler and R. Haupt, in *Quantum Effect Physics, Electronics and Applications*, Proceedings of the International Workshop on Quantum Effect Physics, Electronics and Applications, edited by K. Ismail, T. Ikoma, and H.I. Smith, IOP Conf. Proc. No. 127 (Institute of Physics and Physical Society, London, 1992), p. 51.

[20] L. Wendler, V.G. Grigoryan, and R. Haupt, Superlatt. Microstruct. **12**, 501 (1992).

[21] V. Shikin, T. Demel, and D. Heitmann, Phys. Rev. B **46**, 3971 (1992).

[22] Q.P. Li and S. Das Sarma, Phys. Rev. B **44**, 6277 (1991).

[23] G. Gumbs, D. Huang, and D. Heitmann, Phys. Rev. B **44**, 8084 (1991).

[24] G. Gumbs and D. Huang, J. Phys. C **4**, 1497 (1992).

[25] L. Wendler and V.G. Grigoryan, Phys. Rev. B **49**, 13607 (1994).

[26] A.V. Chaplik and M.V. Krasheninnikov, Surf. Sci. **98**, 533 (1980).

[27] L. Brey, N.F. Johnson, and B.I. Halperin, Phys. Rev. B **40**, 10647 (1989).

[28] F.Y. Huang, J. Phys. C **2**, 5327 (1990).

[29] Hao Chen, Yun Zhu, and Shixun Zhou, Phys. Rev. B **36**, 8189 (1987).

[30] Yun Zhu and Shi-xun Zhou, J. Phys. A **21**, 1361 (1988).

[31] Fengyi Huang, Shengshan Cai, Shi-xun Zhou, and Yun Zhu, J. Phys. D **21**, 375 (1988).

[32] Yun Zhu, Feng-yi Huang, Xiao-ming Xiong, and Shi-xun Zhou, Phys. Rev. B **37**, 8992 (1988).

[33] Yun Zhu, Hao Chen, and Shi-xun Zhou, Phys. Rev. B **38**, 4283 (1988).

[34] D. Huang, Yun Zhu, Z. Lin, and Shi-xun Zhou, Phys. Rev. B **39**, 7713 (1989).

[35] L. Wendler and V.G. Grigoryan, Phys. Status Solidi B **181**, 133 (1994).

[36] U. Merkt, Superlatt. Microstruct. **6**, 341 (1989).

[37] H. Ehrenreich and M.H. Cohen, Phys. Rev. **115**, 786 (1959).

[38] L. Wendler and E. Kändler, Phys. Status Solidi B **177**, 9 (1993).

[39] M. Bonitz, R. Binder, and S.W. Koch, Phys. Rev. Lett. **70**, 3788 (1993).